PROCEEDINGS, 49th Workshop on Geothermal Reservoir Engineering
Stanford University, Stanford, California, February 12-14, 2024
SGP-TR-227

Microseismic Monitoring of a Horizontal EGS System: Case Study and State of the Art

Sireesh DADI, Jack NORBECK, Aleksei TITOV, Travis PAYEUR, Sean MACHOVOE, Kaven JOERN, Kanu CHINAEMEREM

114 Main Street, Suite 200, Houston, Texas 77002

Sireesh.dadi@fervoenergy.com

Keywords: Microseismic, Distributed Acoustic Sensing.

ABSTRACT

In this study, we present the results of microseismic obtained from the stimulation and crossflow activities conducted on two horizontal geothermal wells. Our monitoring approach involved the installation of seismic sensors in both surface and shallow borehole locations, enabling real-time monitoring of seismic activity. Notably, sensors placed on the surface of hard rock formation outcrops exhibited superior signal-to-noise ratios compared to those in shallow boreholes, attributed to the presence of unconsolidated alluvial sands in the shallow subsurface across most of the site. Furthermore, we measured downhole microseismic events using fiber optic cables permanently integrated into four wells. This multi-well fiber optic microseismic acquisition successfully detected approximately 50,000 microseismic events over a three-month monitoring period, a significant increase in detectability compared to the roughly 1,500 detections from the surface and shallow borehole network. However, a challenge in the fiber optic cable acquisition was fiber loss during stimulation due to erosion in poorly cemented areas. The magnitude of events ranged from -2 to 1.5, with the majority falling below 0.5, confidently detected via the fiber optic system. The largest seismic event detected by the surface network registered at magnitude M=1.8 Ml. Importantly, all seismic events remained below the green category threshold established by our Traffic Light System. As a result, no operational changes were required or warranted through all phases of the project to-date, including drilling, stimulation, and well testing. Microseismic events during crossflow remained confined within the stimulated rock volume, exhibiting a direct correlation with reservoir pressure measured by a downhole gauge. This strongly suggests confined crossflow dynamics. Analyzing azimuth data for individual stage events reaffirmed the NE-SW local stress orientation, consistent with the local stress field orientations derived from borehole image log data. In the vertical dimension, microseismic events were symmetrically distributed approximately 300 feet above and below the lateral during the stimulation of the first well. This alignment closely correlated with low-frequency strain rate data from fiber optic observations, indicating fractures extending about 300-500 feet shallower than the stimulation well. Our findings underscore the successful implementation of fiber-based multi-well distributed acoustic sensing (DAS) microseismic monitoring in geothermal fields. Fiber-based microseismic event locations offer insights into crucial fracture geometry parameters, such as fracture orientation, length, and height, as well as microseismic diffusion rates. The absence of reliable three-component borehole tools for operations above 200 °C further underscores the importance of fiber-optic-based microseismic measurements. Enhancements in event resolution and accuracy remain feasible with the incorporation of three-component borehole measurements.

1. INTRODUCTION

Monitoring Enhanced Geothermal Systems (EGS) plays a pivotal role in both predicting and mitigating induced seismicity (Majer et al., 2007; Gaucher et al., 2015; Elsworth et al., 2016; Ree et al., 2021). Additionally, it contributes significantly to reservoir characterization for optimized production (Kim and Avouac, 2023). Traditional methods of microseismic detection in the geothermal industry typically involve the installation of surface or shallow borehole broadband stations. However, given the criticality of understanding fracture parameters in EGS, dedicated monitoring wells are often drilled and equipped with highly sensitive 3C geophones (Kwiatek et al., 2019). Recent experiments conducted at Aalto University's Otaniemi campus in Finland and the Utah FORGE project underscore the evolving landscape of EGS monitoring. In Finland, microseismic monitoring involved an extensive surface network incorporating 3C geophones in a dedicated shallow monitoring zone adjacent to the reservoir (Kwiatek et al., 2019). Meanwhile, the Utah FORGE project, which entailed stimulation in a deviated granite well, boasted a comprehensive monitoring infrastructure. This infrastructure comprised surface broadband stations, surface geophones (Whidden et al., 2023), dedicated deep monitoring wells outfitted with 3C geophones (Rutledge et al., 2022), and the installation of fiber-optic cables within the monitoring wells.

The availability of reliable 3C high-temperature sensors capable of operating in environments exceeding 200°C and continuously recording data for extended periods presents a significant challenge in the geothermal industry. Current market offerings predominantly consist of MEMS-based sensors, whose electronic components are prone to failure at elevated temperatures. Consequently, for the case study discussed in this paper, reliance on fiber optic-based microseismic monitoring was necessitated. The deployment of fiber-optic-based Distributed Acoustic Sensing (DAS) for microseismic monitoring in the geothermal sector is still in its early stages. However, notable progress has been made, particularly demonstrated by the Enhanced Geothermal Systems (EGS) demonstration project at Utah FORGE. Here, downhole fiber optic cable was successfully deployed in the 16B (78)-32 well in 2023, facilitating real-time microseismic monitoring during crossflow tests and future stimulations in 2024. In contrast, the Unconventional Oil and Gas industry has made significant strides in deploying multi-well fiber optic systems for microseismic monitoring and capturing low-frequency strain data to assess fracture hits or Fracture-Driven Interactions (FDI) and stimulated rock volume. For instance, the Hydraulic Fracturing Test Site II (HFTS-2) in the Permian Delaware Basin stands as a comprehensive monitoring program (Ciezobka et al., 2022). By integrating microseismic, low-frequency strain, and pressure gauge data, HFTS-2 aims to advance understanding of fracture hits from child wells to

parent wells and to analyze spatial and temporal reservoir depletion dynamics. These insights gleaned from HFTS-2 hold direct relevance for horizontal EGS systems. Unlike in the context of Oil and Gas production, where fracture hits from child to parent wells are considered detrimental, they are integral to the success of an EGS system.

In this paper, we present a comprehensive case study detailing a multi-well Distributed Acoustic Sensing (DAS) microseismic monitoring program conducted during the stimulation of two horizontal wells in Northern Nevada. We elucidate the methodology wherein permanent fiber optic cables, strategically installed behind the casing in multiple wells, are employed to record microseismic data and facilitate the precise localization of microseismic events. Furthermore, we delve into the application of microseismic data for inferring crucial parameters such as stimulated rock volume, fracture height, and length. Despite the significant potential that multi-well fiber optic systems offer for accurately locating microseismic events, certain challenges persist. These include uncertainties stemming from sub-optimal acquisition practices and the escalating costs associated with deploying and processing DAS-based microseismic data. In this paper, we meticulously examine these challenges, shedding light on the intricacies involved in the acquisition and processing of fiber-based microseismic data. Moreover, we provide insights into the current state-of-the-art methodologies employed to mitigate these challenges and enhance the efficacy of fiber-based microseismic monitoring in geothermal and other subsurface energy applications.

2. WELL FIELD DEVELOPMENT

The wells were drilled as part of a brownfield development adjacent to an existing geothermal plant. This development entailed the drilling of three wells: one vertical monitoring well (73-22), one horizontal injector well (34A-22), and one horizontal producer well (34A-22) (refer to Figure 1). The drilling operations traversed a substantial sedimentary section before reaching the basement rock. A more detailed description of the geology, stress and temperature information of the field is published by Fercho et al., 2023. Each of the three wells is outfitted with permanent instrumentation comprising fiber optic cables installed behind the casing. Additionally, an existing deviated well, 86_22 (depicted in Figure 1), is equipped with fiber optic cable. While the original intent behind installing fiber optic cable in 86_22 was to monitor its stimulation in a pilot project, the same infrastructure was repurposed to monitor the stimulation activities of the horizontal wells.

2.1 Well sequence

The operational sequence commenced with the drilling of the vertical monitoring well, followed by the drilling of the first horizontal well, designated as 34A-22. Subsequently, the stimulation process was initiated, employing a plug-n-perf style completion method comprising sixteen stages. A detailed description of the stimulation style and injection parameters is discussed in Norbeck et al., 2023. Notably, the stimulation treatment involved the pumping of approximately 267,000 barrels (11.2 million gallons) of slickwater fluid and 7.3 million pounds of proppant. Initially, 3C geophones were deployed in the 73-22 well before the commencement of stimulation in 34A-22. However, due to malfunctioning geophones, only a few hours of data were collected. Subsequent microseismic monitoring relied on the downhole permanent fiber optic cable, supplemented by surface and shallow borehole broadband stations. The decision to drill the second horizontal well was informed by the microseismic cloud observed during the stimulation of the first horizontal well, 34A-22. As the drilling of the second well occurred several months after the stimulation of the first well, reservoir pressure had diffused, eliminating any overpressure conditions during the drilling process. During the drilling of the second horizontal well, 34-22, multiple instances of proppant detection from the first well, 34A-22, were noted. Following a six-month interval, the 34-22 well underwent a similar completion style as 34A-22, including stimulation using the plug-n-perf methodology.

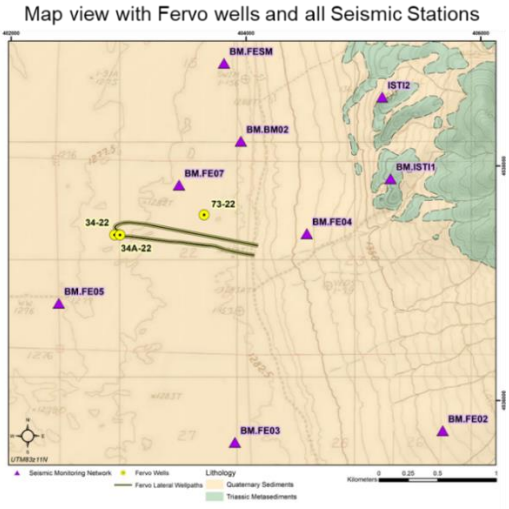

Figure 1: Map view of the three Fervo wells in yellow with the surface and shallow borehole stations installed since June 2020. The 73-22 is the vertical monitoring well and the 34A-22 and 34-22 are the two horizontal injector and producer wells respectively.

The site is equipped with nine broadband seismometers, which have been operational since 2020, allowing for the collection of background seismic data for approximately two years preceding the stimulation of the first horizontal well (refer to Figure 1). Among these

seismometers, two surface stations (ISTI1 and ISTI2) are situated to the east on the mountain, installed within hard rock, while the remaining stations are located in shallow boreholes approximately 50 feet deep. Data collection and processing have been undertaken by the US Geological Survey (USGS) since 2020, spanning the duration from before the stimulation of both horizontal wells. Figure 2 illustrates the seismicity rate per week since the installation of the surface stations. It is noteworthy that all recorded seismicity levels remained below the predefined green threshold limit (<2 Ml) established by the Traffic Light System (TLS).

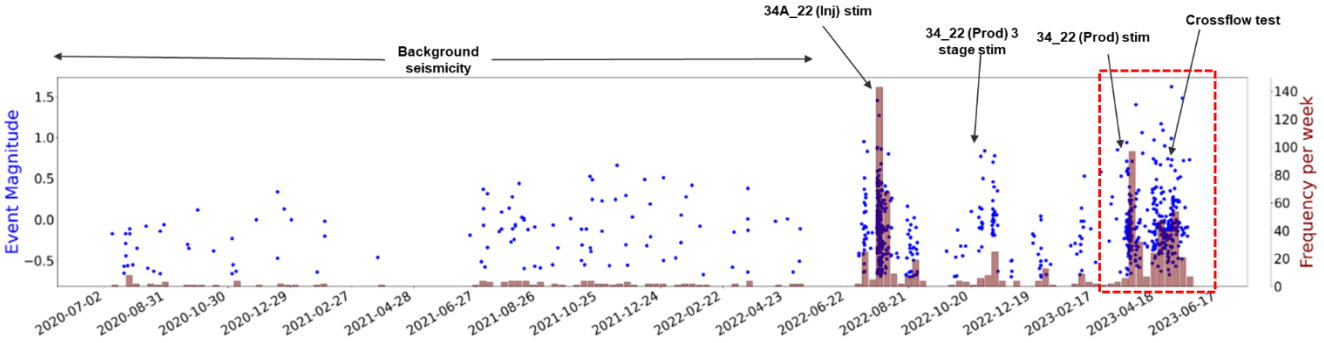

Figure 2: The seismicity rate has been continuously monitored since the deployment of surface/shallow borehole stations in 2020. The network initially collected two years of background seismicity data, which served as a baseline. Subsequently, real-time monitoring of seismicity has been conducted throughout various operations including drilling, stimulation, and crossflow activities. All events included here are M > -0.7 Ml.

2.1 Fiber optic data acquisition

2.1.1 34A-22 Stimulation:

The multi-well microseismic from both the well stimulations was recorded with multiple interrogator units (IU). Three downhole permanent fiber optic cables from three different wells were used for monitoring microseismic for both the stimulations (Table 1 and Figure 3). The permanent fiber optic cable is clamped to the casing while installing the casing downhole (Figure 3b).

During the stimulation of the 34A-22 well, the fiber optic cable experienced erosion after 8 stages, likely due to channeling in the cement that exposed the fiber to higher pressure fluids. Notably, all fiber cables across the wells were equipped with two single-mode fibers and two multi-mode fibers, but one of the single-mode fibers in the 34A-22 well incurred damage during termination at the wellhead. For the stimulation of the first well (34A-22), the interrogator settings were tailored for microseismic monitoring in the single-mode fibers of the 73-22 and 86-22 wells, employing a Gauge Length (GL) of 15 meters. Conversely, data collection from the 34A-22 fiber was optimized for in-well DAS flow allocation at a GL of 5 meters to resolve separate clusters. All data from the interrogators were captured at a sampling rate of 10 kHz. The utilization of a 10 kHz sampling rate and a 5-meter GL proved instrumental in capturing DAS noise along the horizontal section of the 34A-22 fiber. The DAS noise informs the cluster level efficiency of the stages with different completion parameters like number of clusters per stage. Despite the shorter GL of 5 meters, microseismic signals were successfully collected with a favorable Signal-to-Noise Ratio (SNR), as depicted in Figure 4.

A layer cake velocity model was constructed based on the 1D velocity model derived from the dipole sonic data acquired in the 73-22 well (refer to Figure 5a). Given that the 73-22 well was drilled only approximately 200 feet deeper than the horizontal wells, and considering the occurrence of numerous events detected deeper than the sonic log depth interval, the model was extended to deeper depths with a constant value approximating the deeper part of the sonic log value. It's worth noting that the initial perforation shots were not identified on the 73-22 fiber, hindering the calibration of the velocity model. Moreover, continuous seismicity recorded from reservoir stimulation during later stages compounded the challenge of distinguishing perforation shots from background seismicity. Consequently, a grid search-based location method employing waveform stacking was utilized. The majority of events exhibited travel picks closely aligning with the P and S waves on the DAS-triggered microseismic data, suggesting that a smoothed velocity model serves as a satisfactory approximation for event locations (see Figure 5b). For events where no peak was discernible, the depth of the event exceeded the total depth of the fiber. However, when a peak was present, its location provided a close approximation for the event depth, assuming the well was vertical and the medium was isotropic.

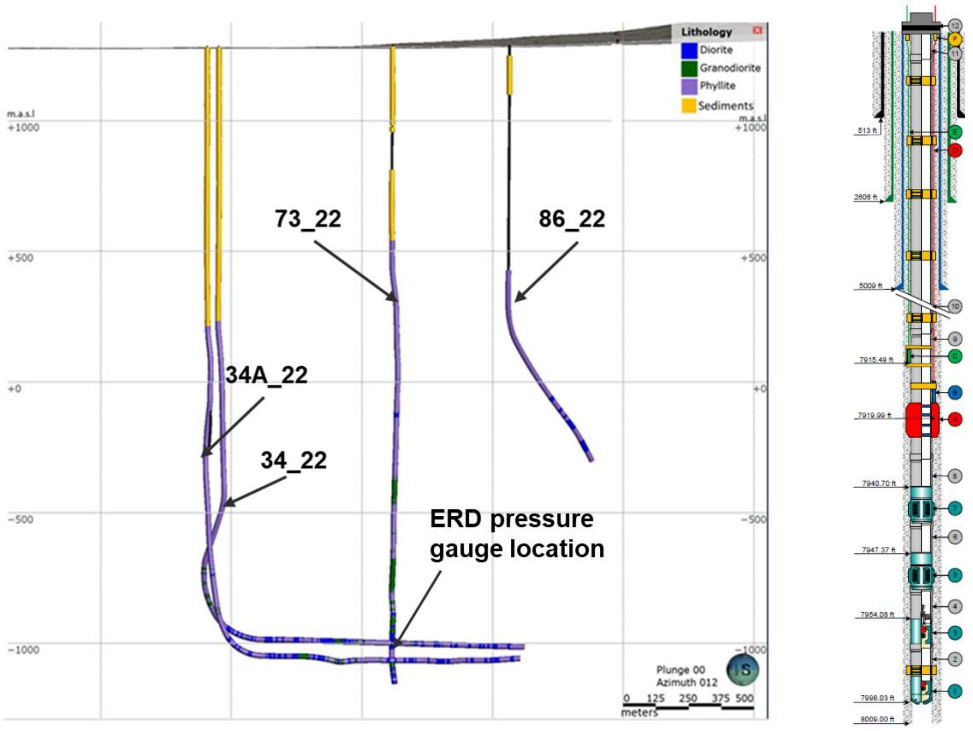

(a) (b)

Figure 3: (a) Cross section view of all four wells installed with permanent fiber optic cable behind casing. 73-22 is the dedicated vertical monitoring well, 34A-22 is the injector and 34-22 is the producer. A map view of these wells is shown in Figure 6 along with the microseismic event locations. (b) Well schematic of the 73-22 well with the red line showing the fiber optic cable installation.

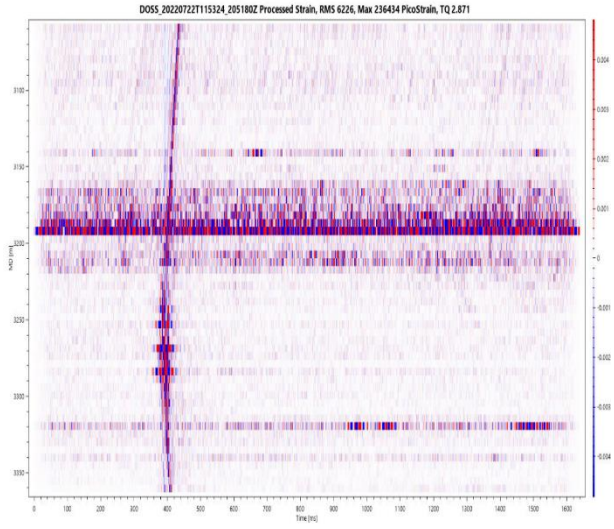

Figure 4: Microseismic event detected on the permanent horizontal fiber installed in 34A-22 during the stimulation. The Gauge Length (GL) for the recording is 5 m and is recording along 300 m section of the fiber. The GL and recording is optimized for in-well DAS flow allocation but the microseismic event with a peak can be identified clearly.

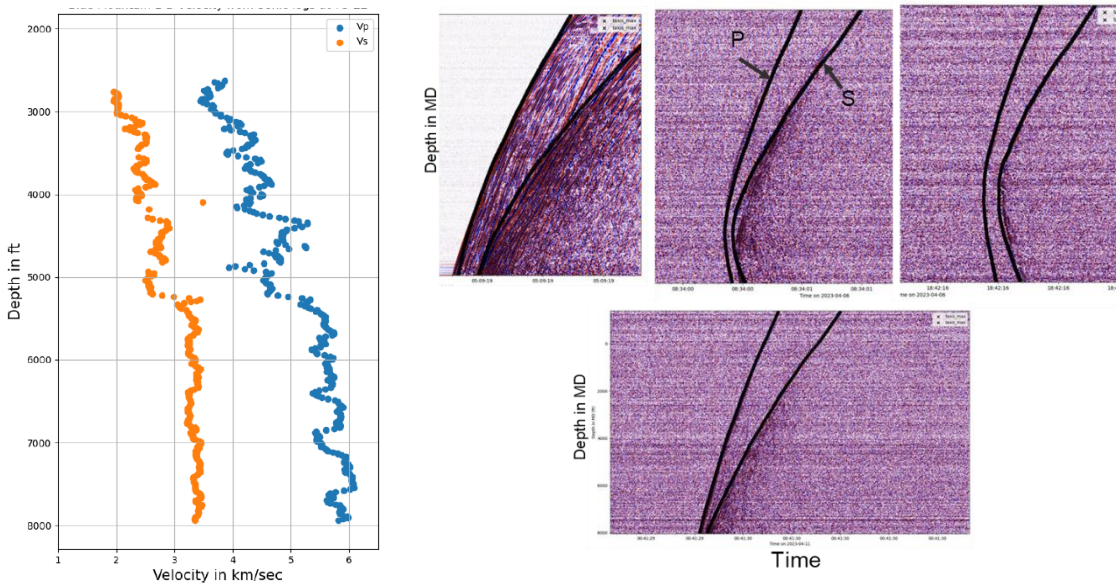

Figure 5: (a) A one-dimensional velocity model derived from the dipole sonic at 73-22. (b) Microseismic data detected on 73-22 fiber with the travel time picks derived from a waveform stacking algorithm at the most likely event locations. The close alignment of the travel time picks with the P and S wave arrivals indicates that the 1D approximation is valid.

The entire microseismic processing suite was outsourced to a third-party vendor, and as a result, the precise details of the processing workflow remain undisclosed. However, it is known that a semblance and modified Short-Term Average/Long-Term Average (STA/LTA) based triggering method was employed initially. This was followed by waveform stacking on a coarser grid, which was subsequently refined at a finer grid scale to enhance the accuracy of event localization.

The stimulation conducted at Injection Well 34A-22 resulted in a significant series of microseismic events, effectively captured by several permanent fiber optic cables with a favorable signal-to-noise ratio. A total of 5,200 events were recorded on the vertical monitoring well, spanning magnitudes from -2 to 1.5. Notably, the majority of these events fell below 0.5 in magnitude, rendering them readily detectable on the fiber. A subset of these events, found within the 5,200 identified on the vertical fiber, were also detected on the horizontal fiber. The integration of data from both fibers markedly bolstered confidence in pinpointing event locations. However, measurements of axial strain along the fibers revealed inherent uncertainty in event locations, particularly within the horizontal planes. The azimuth of individual stage events confirmed the stress orientation in the NE-SW direction as previously identified in various sources across the field (refer to Figure 6). Notably, towards the later stages near the well's heel, a slight rotation of the microseismic cloud towards a more N-S orientation was observed. The event cloud exhibited an approximate extension of 1000 feet in the direction of SHmax, with greater extension observed towards the NE compared to the SW. While it is plausible that events extend symmetrically around the well, those to the south are further from the vertical well and thus more attenuated. Microseismic events displayed a symmetric distribution in the vertical direction, extending approximately 300 feet above and below the stimulated well. These events were also discernible as stripes in the low-frequency strain rate data. A notable correlation was observed between the height of microseismic events and the observed extension in the low-frequency strain rate data, suggesting that fractures extended approximately 300-500 feet shallower than the treatment well (Titov et al., 2024). However, the absence of fiber below the horizontal well precluded drawing similar conclusions at deeper levels. Nonetheless, the microseismic data indicated that fractures did indeed extend approximately 300 feet deeper.

Map View of 34A-22 microseismic events

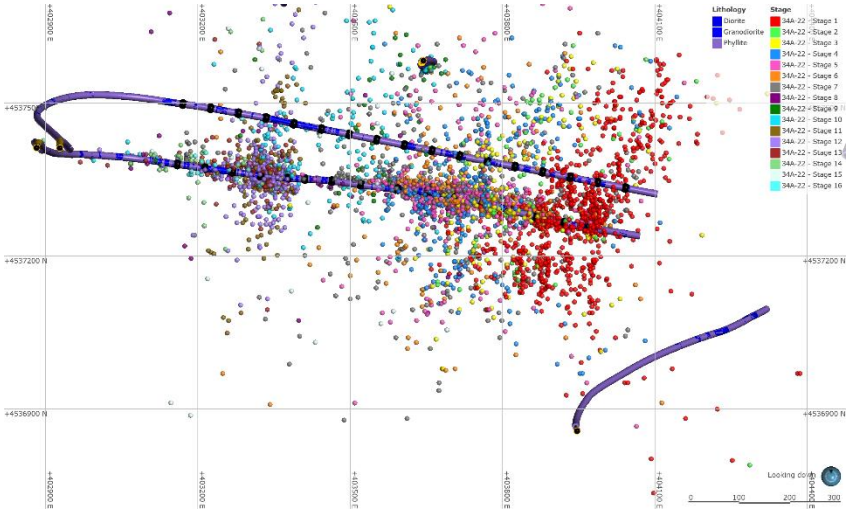

Cross section view of 34A-22 microseismic events

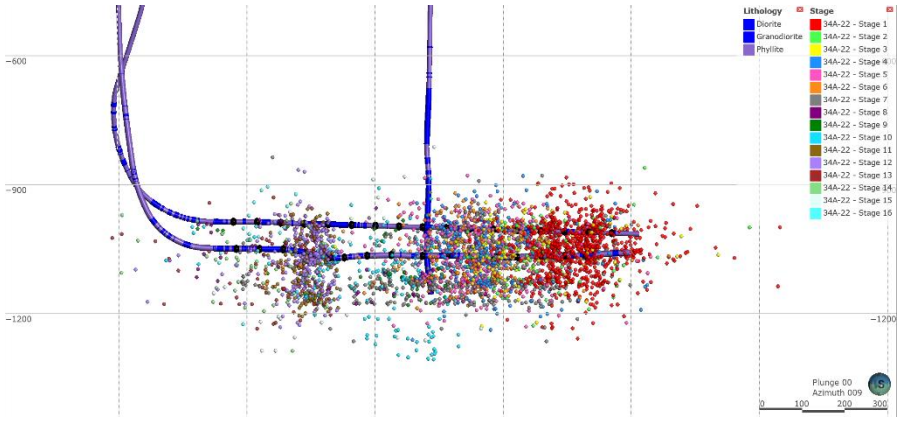

Figure 6: (a) Map view and (b) cross section view of the microseismic events during the 34A-22 stimulation obtained from DAS based microseismic collected in 73-22, 86-22 and 34A-22 fibers. The events are color coded with the stage numbers.

2.1.2 34-22 Stimulation:

The stimulation campaign for well 34-22 commenced in October 2022 with an initial three-stage treatment, which was later postponed to January 2023 due to operational reasons. The entire well was successfully stimulated in January 2023. Table 1 provides a comparative analysis of the microseismic acquisition parameters, and the live fibers utilized for microseismic processing during the stimulation of both wells. During the 34-22 stimulation, both single-mode fibers remained operational, facilitating the collection of microseismic data along the entire length of the fiber until its eventual failure. However, the horizontal fiber in the 34-22 well experienced failure at the end of the vertical section during the October 2022 stimulation, following completion of the first stage. A concentration of events was observed near the toe of the 34-22 well during the October 2022 stimulation, as depicted in Figure 7. The event showcased in Figure 7 occurred near the well's toe and exhibited sufficient magnitude to be recorded across the entire length of the 34-22 fiber, spanning the horizontal, curve, and vertical sections. The near-zero P and S wave separation observed on the 34-22 fiber indicated the event's proximity to the well. Additionally, the P-wave detected at the 73-22 well arrived nearly perpendicular to the well. Given that Distributed Acoustic Sensing (DAS) records only axial movements along the fiber and considering the perpendicular particle motion of the P-wave to the well, the amplitude of the P-wave approached zero in the 73-22 fiber data (refer to Figure 7).

Table 1: List of active fibers used for monitoring the 34-22 and 34A-22 stimulations and DAS microseismic acquisition parameters.

Well	Active fibers used for microseismic monitoring			Acquisition Frequency	Gauge length	Channel spacing
34A-22 stimulation	73-22 to total depth	34A-22 entire fiber for 10 stages. 34A-22 fiber to 8620 ft after 8th stage.	86-22 to total depth	10000 Hz	15 m	1 m
34-22 stimulation	73-22 to total depth	34A-22 fiber to 8620 ft.	86-22 to total depth	10000 Hz	15 m	1 m

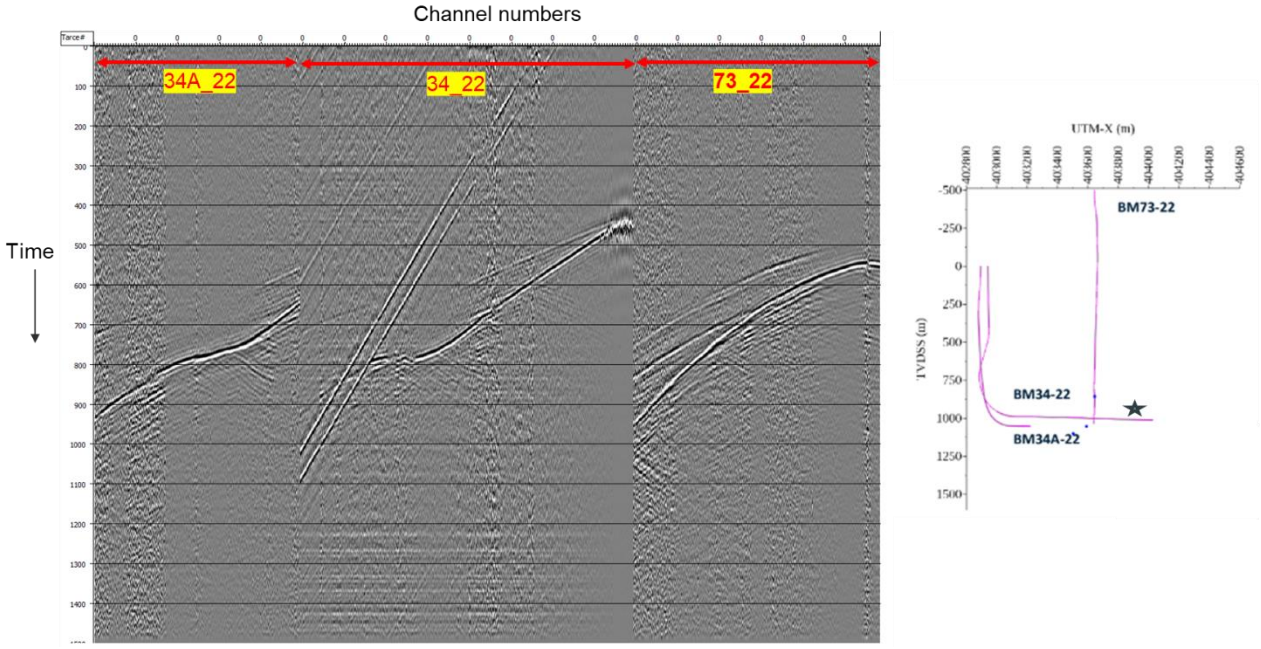

Figure 7: Microseismic data of one of the events which occurred near the toe of the 34-22 well. The seismic data is a combined triggered harvested file from all the fibers together. The x-axis shows the channel numbers of the fibers, and the y-axis is in time. The well plot to the right shows all the live fibers when the microseismic event occurred.

For events detected on all three fibers (73-22, 86_22, and 34A-22), the uncertainty in event location can be significantly reduced to a single distinct region, as illustrated in Figure 8. The fiber in the 73-22 well plays a crucial role in estimating the depth of the event, while the fibers in the 34A-22 and 86_22 wells contribute to determining the aerial location of the event. However, certain events triggered were either not detected on the 86_22 fiber or the 34A-22 fiber exhibited excessive noise due to fluid injection-related tube wave noise. In such instances, the event location can only be identified with a degree of uncertainty, typically represented by two distinct regions, as depicted in Figure 9. The uncertainty becomes evident when analyzing microseismic event locations on a stage-by-stage basis. For instance, during stage 10 when stimulation is closest to the 73-22 well and numerous events are detected in both the 34A-22 and 86_22 fibers, the event locations are well constrained, showcasing a microseismic cloud oriented along the Shmax orientation, as shown in Figure 10a. However, during stimulation stages near the heel, the lack of detections on the 86_22 fiber contributes to increased uncertainty in event location, resulting in a dominant NE-SW and NW-SE trend in the microseismic cloud, as depicted in Figure 10b. Despite the presence of a dominant NW-SE trend in the microseismic cloud during stage 18 of the 34-22 stimulation, there is no indication of any dominant axial or NW-SE fracture network near the wellbore when history matching the stimulation and crossflow results in the reservoir model. This suggests that the NW-SE trend observed in the microseismic cloud during stage 18 may be an artifact.

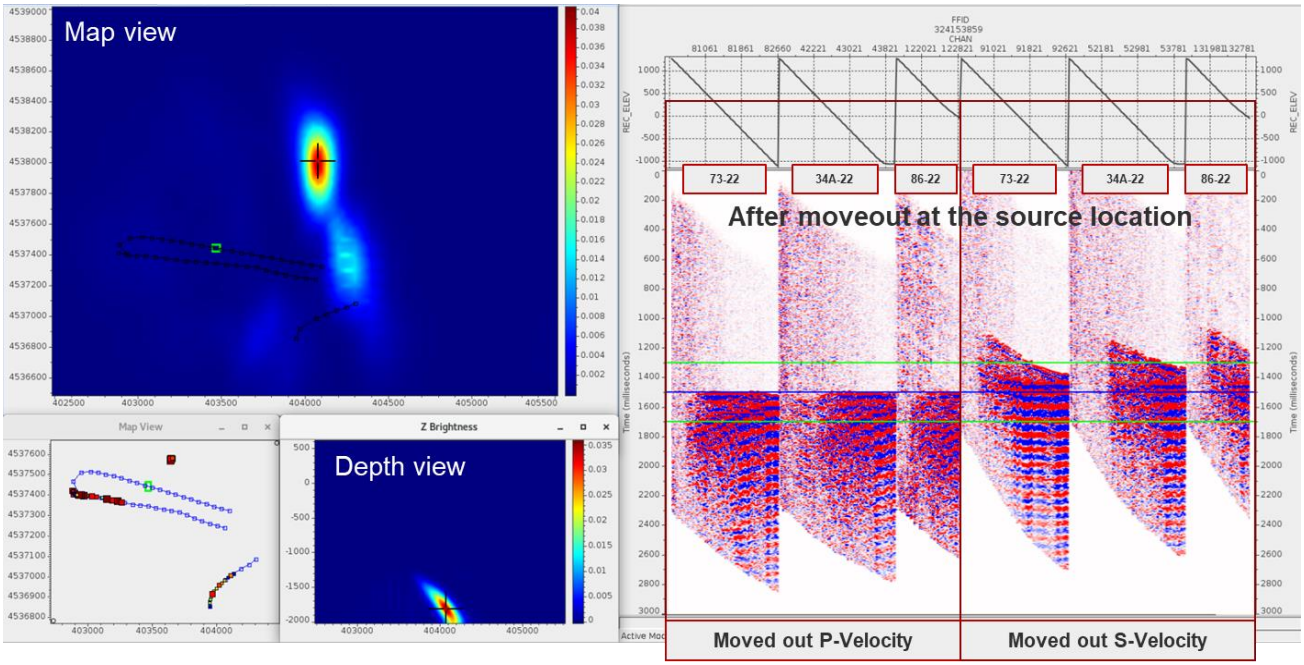

Figure 8: The 2D map and depth cross section energy plots of a microseismic event obtained after a course grid search followed by a recursive fine grid search. For each grid point the events of the microseismic data are flattened based on pre calculated travel time grid. The point in the grid with the highest energy is defined as the source microseismic location.

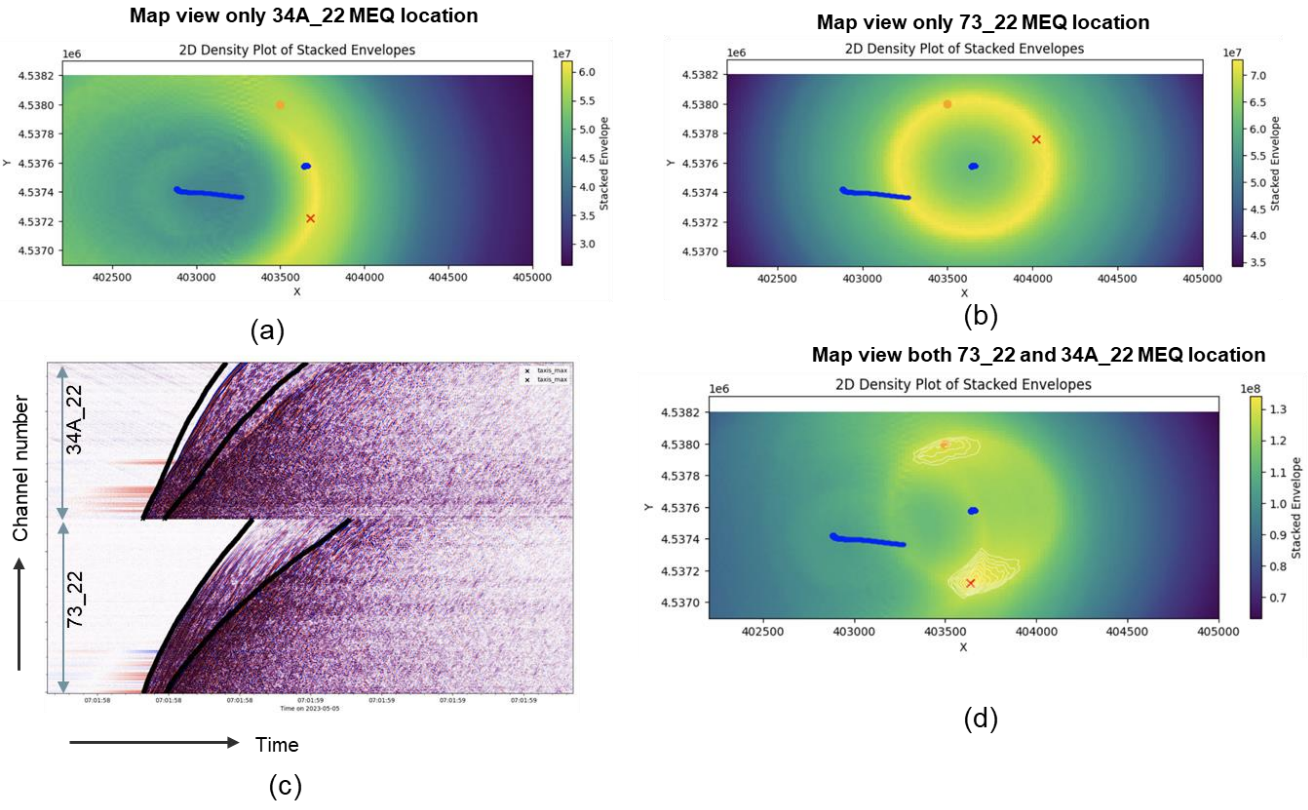

Figure 9: Microseismic event location based on only two fibers in 73-22 and 34A-22 without the 86-22 fiber data. The blue dots show the live fiber when the microseismic is collected. (a) Map view of the event location based only on the fiber data from 34A-22. (b) Map view of the event location based only on the fiber data from 73-22. (c) DAS microseismic data overlaid with the travel picks of the most likely source location (d) An energy plot derived from both fibers is presented, which reduces the location uncertainty to two points, indicating a narrowing of the uncertainty from a donut-shaped distribution.

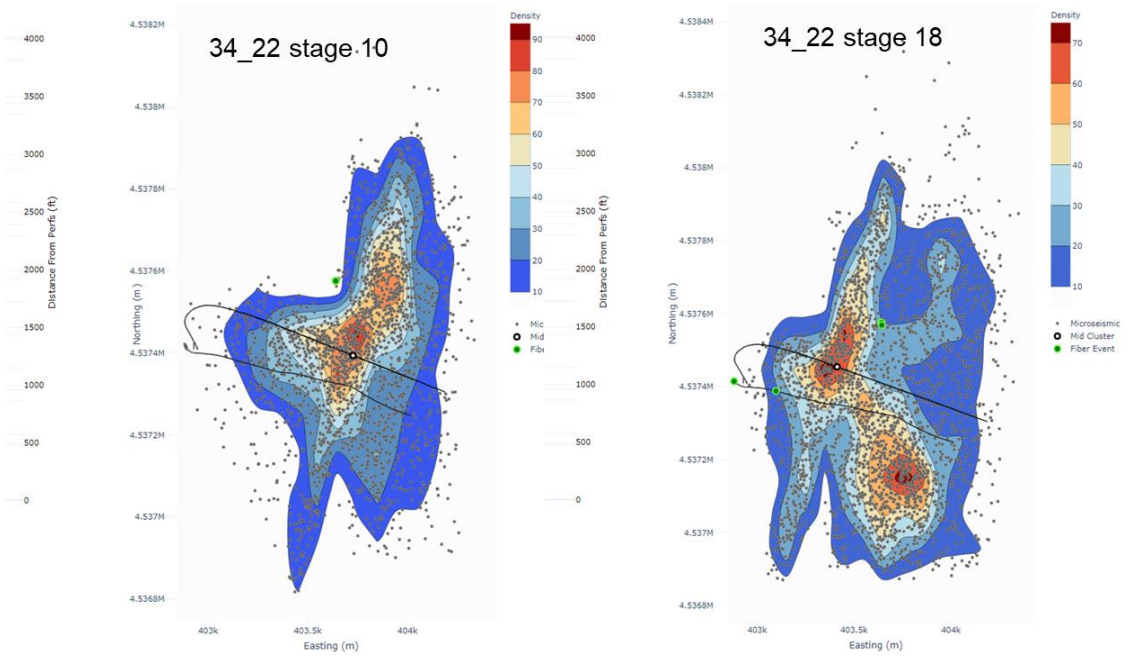

(a) (b)

Figure 10: (a) Microseismic cloud of stage 10 during the stimulation of 34-22 well. b) Microseismic cloud of stage 18 during the stimulation of 34-22 well.

The three stages near the toe of the 34-22 well underwent stimulation twice for operational reasons, the details of which are not discussed here. This double stimulation is clearly evident in the microseismic cloud obtained during the 34-22 stimulation in January 2023, as depicted in Figure 11. Notably, a dominant cloud oriented in the NE-SW direction, closer to the SHmax orientation, is observed. The size of the microseismic cloud expanded towards the north of the well doublet and in depth, both above and below the horizontal wells. This expansion may be attributed to the reactivation of previously created fractures from the 34A-22 stimulation and the creation of new fractures during the 34-22 stimulation. In both well stimulations, the number of events is influenced by the proximity of the stage to the 73-22 well, resulting in a bias in event detection, as illustrated in Figure 12a. The detections from the 73-22 well are dominant compared to those from the 86_22 well and the remaining fibers in the horizontal wells. This dominance can be attributed to the dedicated monitoring nature of the 73-22 well compared to the horizontal wells, which are subject to fluid injection noise, and the 86_22 well, which is shallower and located away from the doublet wells. Additionally, during the 34-22 stimulation, there is a higher number of events recorded at deeper levels compared to the 34A-22 stimulation.

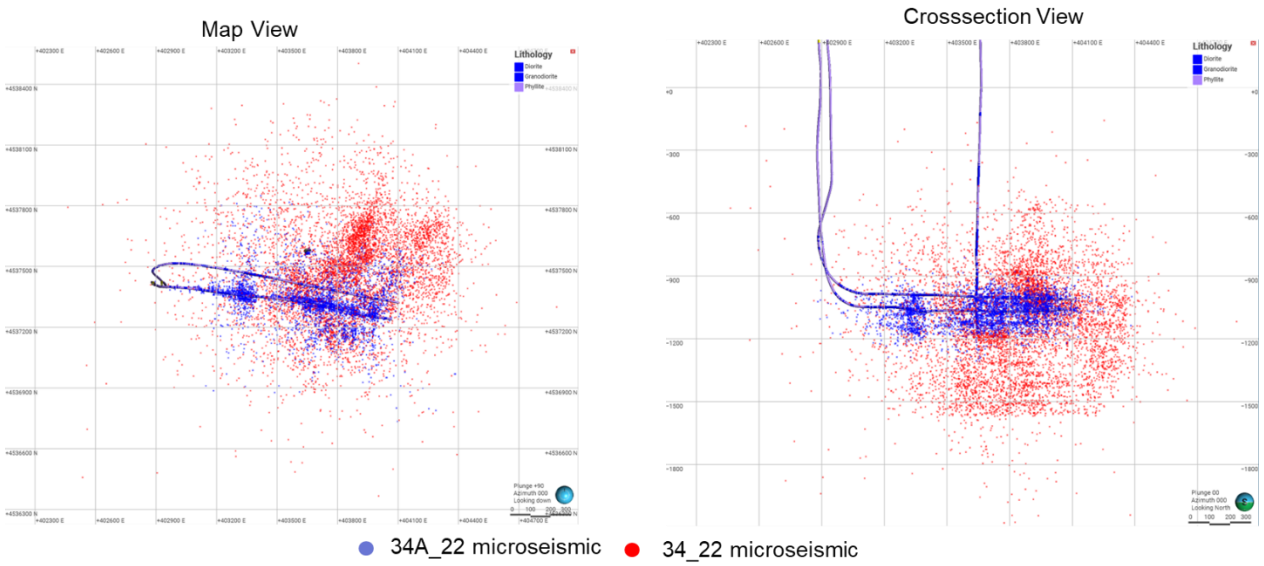

Figure 11: Map and cross section view of the microseismic clouds from both the 34A-22 and 34-22 stimulations together.

The analysis of microseismic data from the stimulation of both horizontal wells indicates a lower frequency of events near the heel stages. The estimated range of the half fracture length and half height for the 34-22 stimulation are approximately 1000 feet and 800 feet, respectively, near the toe, and around 600 feet and 250 feet, respectively, near the heel stages (refer to Figures 12b and 12c). Notably, the microseismic cloud from both wells demonstrates the feasibility of creating an effective fracture network in basement rocks. To measure injection flow rates in the 34A-22 well, a spinner log accompanied by a fiber optic cable was deployed in the 34A-22 injector well (as detailed by Norbeck & Latimer., 2023). The spinner log provided direct measurements of flow rates across all stages between the wells, without any significant bias towards a few connecting hydraulic fractures. Moreover, the accompanying wireline fiber optic cable enabled the derivation of flow rates and temperatures. An ensemble of reservoir models was employed to simulate scenarios where fractures propagate downward, as opposed to shallower propagation due to decreasing stress fields at shallower depths. One such scenario involves cooler fluids descending initially due to higher density, subsequently cooling the rock and causing shrinkage, thereby reducing stress and resulting in downward propagation of fractures. McClure (2023) investigated how fracture opening and buoyancy-driven fluid circulation contribute to downward fracture propagation during long-term circulation, significantly enhancing the thermal longevity of the system.

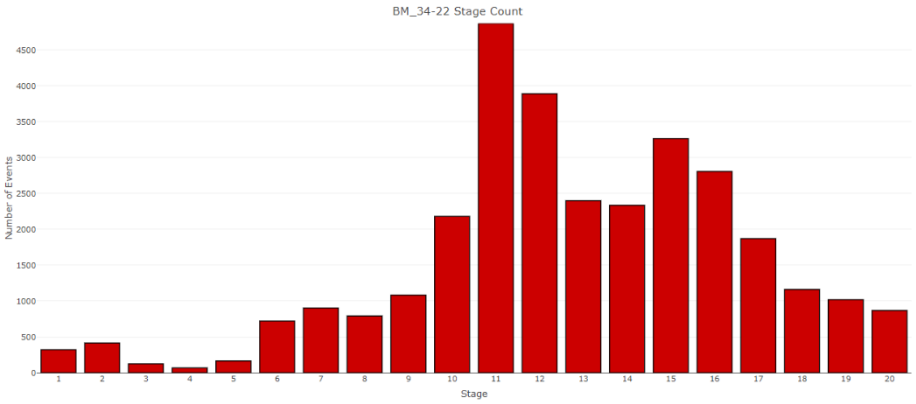

(a)

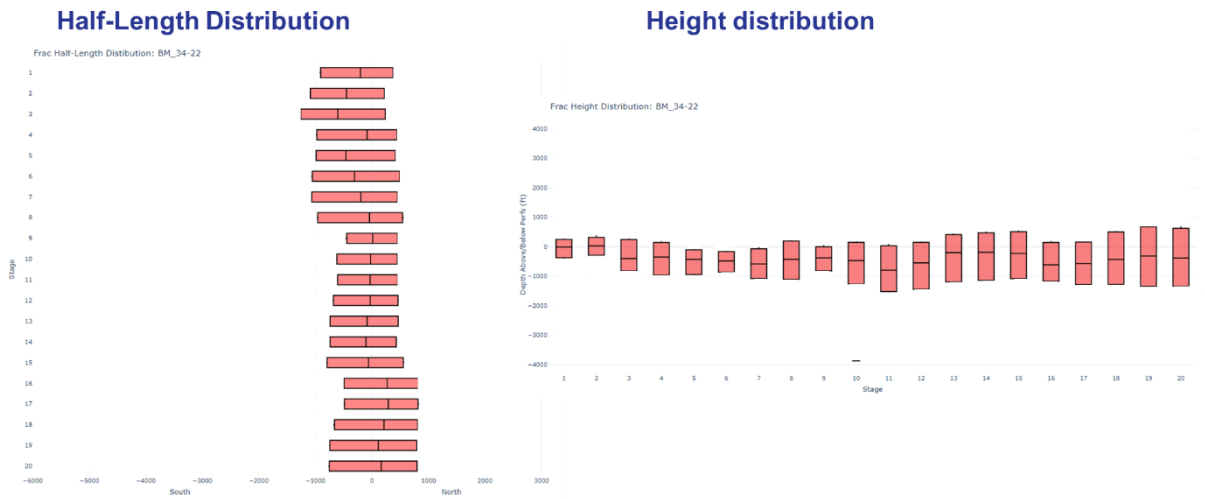

(b) (c)

Figure 12: (a) Number of microseismic events detected on the 73-22 fiber per stage. There is a detection bias depending on the proximity of the stage to the 73-22 fiber. (b) Frac half length box plot for all stages during the 34-22 stimulation (c) Frac half height box plot for all stages during the 34-22 stimulation.

2.1.2 Seismicity during crossflow test:

Following the stimulation of the 34-22 well, a crossflow test was conducted between the two wells for approximately 40 days to establish flow between them. The primary objective of the crossflow test was to achieve steady-state performance with commercial quantities of flow between the wells and to conduct a series of load-following dispatchability tests (refer to Norbeck and Latimer, 2023). Real-time monitoring of seismicity was conducted using both the surface station network and the downhole permanent fiber optic cables in wells 73-22 and 34A-22. The seismicity observed in the 73-22 well (illustrated by the red histograms in Figure 13) exhibited a strong

correlation with the pressure measurements obtained from an Electrical Resonating Diaphragm (ERD) gauge installed behind the casing in the 73-22 well at the reservoir location (as depicted in Figure 3a). This pressure gauge, installed outside the casing and permanently cemented, directly measures reservoir pressure. It is noteworthy that the number of events detected on the downhole permanent fiber cable in the 73-22 well was approximately 60-70 times greater than the events detected on the surface. Furthermore, the observed seismicity remained below magnitude 2, which aligns with the green threshold limit in the Traffic Light system. An ongoing research effort focuses on estimating magnitudes from fiber optic-based detections, akin to the work conducted by Yin et al. (2023). This involves developing a data-driven method to establish the scaling relation between Distributed Acoustic Sensing (DAS) amplitude and earthquake magnitude observed on surface stations. However, a key challenge lies in accounting for attenuation corrections due to the location disparity between surface stations and downhole fiber optic cables. It is important to note that all observed seismicity during the crossflow test remained within the previously stimulated area. As the pressure dissipated following the conclusion of the crossflow test in May 2023, seismicity decreased accordingly. Although the relationship between seismicity and pressure diffusion during load dispatchable cycles around May 5th, 2023, is not explored in this paper, a more detailed study on this topic is planned for future publication.

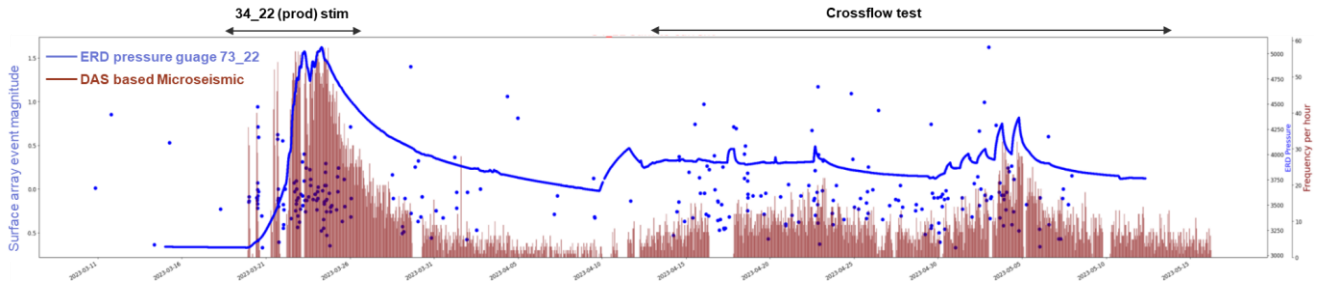

Figure 13: Seismicity rate derived from the DAS based microseismic data during the 34-22 stimulation in January 2023 until the end of the crossflow test in April-May 2023.

3. STATE OF THE ART AND CHALLENGES

3.1 Microseismic Acquisition

A critical aspect of accurately locating microseismic events lies in optimizing the acquisition process. Traditionally, the geothermal industry has relied on surface seismic measurements, including broadband sensors and passive seismic emissions, to monitor seismicity. However, in prolific geothermal provinces like the Western US, the presence of shallow unconsolidated sediments leads to severe scattering attenuation, posing challenges in achieving good Signal-to-Noise Ratio (SNR) in seismic data collected at surface stations. In contrast, the Unconventional Oil and Gas industry utilizes 3C geophones, often rated for temperatures below 180°C, to obtain high-resolution microseismic events. However, as most of the reservoirs targeted by the geothermal industry intentionally operate at temperatures greater than 200°C, the 3C sensors commonly deployed in the Oil and Gas sector are not suitable. To address this technological gap, the Geothermal Technology Office (GTO) has initiated the Geothermal Geophone Prize, sponsoring companies to manufacture all-temperature 3C geophones (herox.com/GeophonePrize). Although this initiative is commendable, the availability of final Phase 3 funding is not expected until 2025, thus indicating a technology gap in the near future. Furthermore, a challenge for deploying 3C high-temperature geophones lies in the conveyance method for tools in boreholes. Currently, there are no tractors available in the market suitable for operating temperatures greater than 200°C. Consequently, even if 3C geophones become available, their deployment would be limited to vertical and deviated wells, excluding horizontal wells. Given these challenges, it is imperative for the geothermal industry to collaborate effectively. This collaboration could involve concerted efforts from the GTO office, sensor and wireline companies, and multiple operators, possibly through a consortium. Such collaborative endeavors aim to make 3C sensor technology available at a reasonable cost and at scale for the geothermal industry.

The advancements in fiber optic technology, driven primarily by the Oil and Gas industry, present significant opportunities for the geothermal sector. The integration of Distributed Acoustic Sensing (DAS)-based microseismic and low-frequency DAS (or high-resolution Distributed Strain Sensing) information, along with temperature sensing capabilities provided by Distributed Temperature Sensing, offers a wealth of valuable data at a competitive acquisition cost (e.g., Titov et al., 2023). Various types of fiber optic deployments hold potential value for the geothermal industry. These include permanent fiber optic cables deployed behind the casing, temporary wireline encapsulated fiber optic cables, single-use fiber optic cables, and wireline fiber optic cables integrated with 3C geophone sensors (referred to as a hybrid fusion array). Permanent fiber optic cables are readily available in the market, offering high-quality data recording capabilities. However, high-temperature temporary options pose challenges due to manufacturing and supply chain constraints, insufficient demand at scale, and, more importantly, a degradation in data quality due to poor coupling with the host rock compared to the permanent fiber (LeBlanc et al., 2023). As the Enhanced Geothermal Systems (EGS) industry matures and expands, temporary fiber optic solutions are expected to gain momentum. Temporary fibers offer the advantage of not requiring well design changes and can be deployed within the casing, facilitating monitoring in multiple wells. Among temporary options, deploying a wireline with fiber optic sensors integrated with a 3C geophone or optical accelerometer array (the hybrid fusion array) stands out as a promising choice. This setup can be scaled for monitoring tens of wells and hundreds of stages, providing real-time data during operations. The hybrid fusion array, when deployed in an adjacent horizontal monitoring well, can be moved stage by stage in sync with

a nearby stimulated well. This setup enables the collection of valuable low-frequency strain data, which can inform on fracture hits or Fracture Driven Interactions (FDI). Despite its promise, the hybrid array faces challenges, including the lack of high-temperature tractors for deploying and moving attached sensors, as well as the complexity of incorporating high-temperature fibers into the wireline. Addressing these challenges will be crucial for realizing the full potential of this technology in the geothermal industry.

Table 2: Comparison of monitoring tools for Enhanced Geothermal systems, their advantages, disadvantages, and current technology status. * Number of Y's describe the level of spatial resolution achievable with the proposed technology. It is a relative score. ** Number of $'s describes the cost of the technology for deploying at scale.

	Technology readiness level	Temperature profiling	SRV (Stimulated rock volume)	Cost of deployment	Production profiling	Frac hit/FDI	Well integrity
3C Geophones	NA	N	YYYY*	$$$$$**	N	N	N
Permanent fiber	Y	Y	YYY	$$$$$	Y	Y	Y
Temporary fiber	NA	Y	YY	$$$	Y	Y	N
Temporary Hybrid fiber + 3C geophones	NA	Y	YYYY	$$	N	Y	N
Surface Geophones	Y	N	Y	$	N	N	N
Tracer	Y	N	Y	$	Y	N	N
SWPM (Sealed wellbore pressure monitoring) (Haustveit et al 2020)	Yes, but may not be feasible due to large diameter (7" or larger)	N	Y	$	N	Y	N

3.2 Microseismic Processing

With the advent of large-scale computing capabilities, real-time processing of microseismic events with fiber optic data has become possible. There have been significant advances in triggering, phase picking, and the localization of microseismic events using fiber optic data. This paper specifically addresses the challenges associated with phase picking. PhaseNet (Zhu and Beroza, 2019) and various machine-learning-enabled models for phase or first arrival picking have proven effective in accelerating the estimation of seismic phase arrivals from earthquakes or microseismic events. These machine learning models play a critical role, especially in estimating travel times on dense Distributed Acoustic Sensing (DAS) datasets. Recently, Zhu et al. (2023) used semi-supervised learning to develop a model for dense DAS arrays. However, there is still a need to expand model building to various DAS data across a range of subsurface models. Some of the current challenges associated with the use of machine learning models are highlighted in Figure 14.

4. CONCLUSION

The successful implementation of fiber-based multi-well Distributed Acoustic Sensing (DAS) microseismic monitoring within the Enhanced Geothermal Systems (EGS) field marks a significant milestone in our understanding of fracture geometry parameters critical for optimizing geothermal reservoir performance. Despite the absence of reliable three-component borehole tools capable of operating at temperatures exceeding 400 °F, fiber-optic-based microseismic measurements have emerged as a cornerstone in providing invaluable insights into fracture orientations, lengths, heights, and propagation rates. Our proof-of-concept study has demonstrated the efficacy of fiber-based DAS technology in characterizing geothermal reservoirs, showcasing its potential to revolutionize reservoir management practices in the field. Looking ahead, future research efforts should be directed toward refining and advancing more fiber-based acquisition microseismic monitoring techniques. This includes developing innovative methods for mitigating fiber cable failures, enhancing data processing algorithms to improve accuracy and resolution, and integrating temporary fiber optic cable monitoring technologies for comprehensive reservoir characterization.

4. ACKNOWLEDGEMENTS

This work is partially funded through the US Department of Energy (DOE) ARPA-E under Award No. DE-AR001604

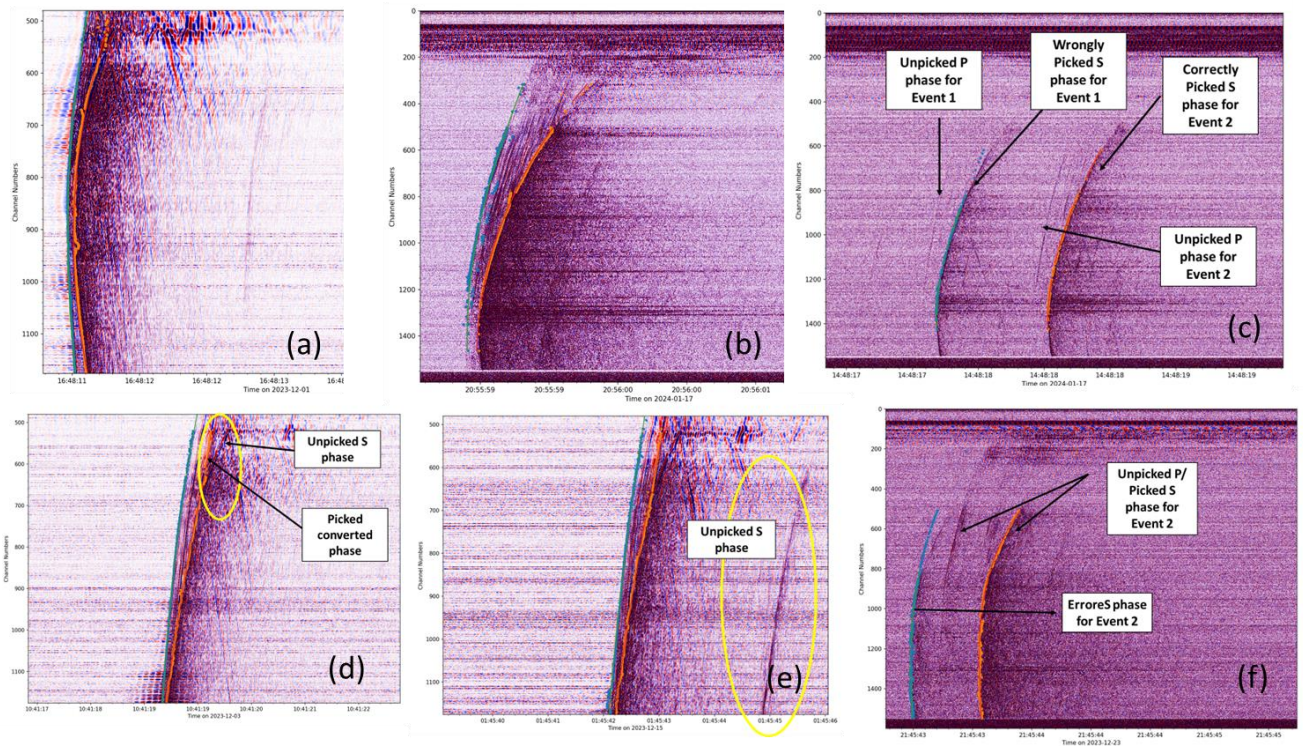

Figure 14: (a) and (b) show images of P and S picks on microseismic events when PhaseNet performed well. (c) – (f) are events when either there are mis picks or when picks are not picked. In this figure, some converted phases are mistakenly picked as the first arrival S. Occasional omission of weak events among a group of events within a record. Erroneous phase picks when some phases are not recorded in the data. For example, in Figure f, the S phase was incorrectly picked as a P phase due to missing P phases in the data.

REFERENCES

Ciezobka J. Overview of Hydraulic Fracturing Test Site 2 in the Permian Delaware Basin (HFTS-2). InUnconventional Resources Technology Conference, 26–28 July 2021 2021 Dec 1 (pp. 259-278). Unconventional Resources Technology Conference (URTeC).

Chavarria JA, Oukaci Y, Laflame L. Multiwell DAS Microseismic and Strain Measurements Diagnostics. InARMA US Rock Mechanics/Geomechanics Symposium 2022 Jun 26 (pp. ARMA-2022). ARMA.

Elsworth D, Spiers CJ, Niemeijer AR. Understanding induced seismicity. Science. 2016 Dec 16;354(6318):1380-1.

Fercho S, Norbeck J, McConville E, Hinz N, Wallis I, Titov A, Agarwal S, Dadi S, Gradl C, Baca H, Eddy E. Geology, State of Stress, and Heat in Place for a Horizontal Well Geothermal Development Project at Blue Mountain, Nevada. InProceedings, 48th Workshop on Geothermal Reservoir Engineering, Stanford University, Stanford, CA 2023 Feb.

Gaucher E, Schoenball M, Heidbach O, Zang A, Fokker PA, van Wees JD, Kohl T. Induced seismicity in geothermal reservoirs: A review of forecasting approaches. Renewable and Sustainable Energy Reviews. 2015 Dec 1;52:1473-90.

Haustveit K, Elliott B, Haffener J, Ketter C, O'Brien J, Almasoodi M, Moos S, Klaassen T, Dahlgren K, Ingle T, Roberts J. Monitoring the pulse of a well through sealed wellbore pressure monitoring, a breakthrough diagnostic with a multi-basin case study. InSPE Hydraulic Fracturing Technology Conference and Exhibition 2020 Jan 28 (p. D021S004R001). SPE.

Kim T, Avouac JP. Stress-Based and Convolutional Forecasting of Injection-Induced Seismicity: Application to the Otaniemi Geothermal Reservoir Stimulation. Journal of Geophysical Research: Solid Earth. 2023 Apr;128(4):e2022JB024960.

Kwiatek G, Saarno T, Ader T, Bluemle F, Bohnhoff M, Chendorain M, Dresen G, Heikkinen P, Kukkonen I, Leary P, Leonhardt M. Controlling fluid-induced seismicity during a 6.1-km-deep geothermal stimulation in Finland. Science Advances. 2019 May 1;5(5):eaav7224.

Majer EL, Baria R, Stark M, Oates S, Bommer J, Smith B, Asanuma H. Induced seismicity associated with enhanced geothermal systems. Geothermics. 2007 Jun 1;36(3):185-222.

Mantell ME, Mercer A, Jackson JB, Murphy DJ, Conaway J, Machovoe SR, Stokes J, Elliott M. Application of disposable fiber technology to evaluate far-field communication and fracture performance in the Marcellus Shale. InSPE Hydraulic Fracturing Technology Conference and Exhibition 2022 Jan 25 (p. D011S002R004). SPE.

McClure M. Thermoelastic fracturing and buoyancy-driven convection: Surprising sources of longevity for EGS circulation. arXiv preprint arXiv:2308.02761. 2023 Aug 5.

Norbeck J, Latimer T, Gradl C, Agarwal S, Dadi S, Eddy E, Fercho S, Lang C, McConville E, Titov A, Voller K. A Review of Drilling, Completion, and Stimulation of a Horizontal Geothermal Well System in North-Central Nevada. InProceedings, 48th Workshop on Geothermal Reservoir Engineering, Stanford University, Stanford, CA 2023.

Norbeck JH, Latimer T. Commercial-scale demonstration of a first-of-a-kind enhanced geothermal system. 2023 https://doi.org/10.31223/X52X0B

LeBlanc M, Suh K, Machovoe S, Byrd D, Jaaskelainen M, Bland H, Stokes J, Henao T, Sahdev N. Theory and Practice of a Flexible Fiber-Optic Cable in a Horizontal Well Used for Crosswell and Microseismic Hydraulic Fracture Monitoring. SPE Journal. 2023 Jun 14;28(03):1453-69.

Ree JH, Kim KH, Lim H, Seo W, Kim S, An X, Kim Y. Fault reactivation and propagation during the 2017 Pohang earthquake sequence. Geothermics. 2021 May 1;92:102048.

Rutledge J, Dyer B, Bethmann F, Meier P, Pankow K, Wannamaker P, Moore J. Downhole microseismic monitoring of injection stimulations at the Utah FORGE EGS Site. In ARMA US Rock Mechanics/Geomechanics Symposium 2022 Jun 26 (pp. ARMA-2022). ARMA.

Titov A, Norbeck J, Dadi S, Voller K, Woitt M, Fercho S, McConville E, Lang C, Agarwal S, Gradl C, Latimer T. Case Study: Completion and Well Placement Optimization Using Distributed Fiber Optic Sensing in Next-Generation Geothermal Projects. InSPE/AAPG/SEG Unconventional Resources Technology Conference 2023 Jun 13 (p. D031S057R001). URTEC.

Titov, A., Dadi, S., Galban, G., Norbeck, J., Almasoodi, M., Pelton, K., Bowie, C., Haffener, J. and Haustveit, K. Optimization of Enhanced Geothermal System Operations Using Distributed Fiber Optic Sensing and Offset Pressure Monitoring. In SPE Hydraulic Fracturing Technology Conference and Exhibition. 2024

Whidden KM, Petersen G, Pankow KL. Seismic Monitoring of the 2022 Utah FORGE Stimulation: The View from the Surface.

Yin J, Zhu W, Li J, Biondi E, Miao Y, Spica ZJ, Viens L, Shinohara M, Ide S, Mochizuki K, Husker AL. Earthquake Magnitude With DAS: A Transferable Data-Based Scaling Relation. Geophysical Research Letters. 2023 May 28;50(10):e2023GL103045.

Zhu W, Beroza GC. PhaseNet: A deep-neural-network-based seismic arrival-time picking method. Geophysical Journal International. 2019 Jan;216(1):261-73.